Received: 25 April 2022 | Revised: 14 July 2022 | Accepted: 9 August 2022

DOI: 10.1111/ffe.13816

ORIGINAL ARTICLE

FFEMS Fatigue & Fracture of Engineering Materials & Structures WILEY

Effect of microstructural heterogeneity on fatigue strength predicted by reinforcement machine learning

Mustafa Awd[1] | **Sebastian Münstermann**[2] | **Frank Walther**[1]

[1]Chair of Materials Test Engineering (WPT), TU Dortmund University, Dortmund, Germany

[2]Integrity of Materials and Structures, Steel Institute, RWTH Aachen University, Aachen, Germany

Correspondence
Mustafa Awd, Chair of Materials Test Engineering (WPT), TU Dortmund University, Baroper Str. 303, D-44227, Dortmund, Germany.
Email: mustafa.awd@tu-dortmund.de

Abstract

The posterior statistical distributions of fatigue strength are determined using Bayesian inferential statistics and the Metropolis Monte Carlo method. This study explores how structural heterogeneity affects ultrahigh cycle fatigue strength in additive manufacturing. Monte Carlo methods and procedures may assist estimate fatigue strength posteriors and scatter. The acceptable probability in Metropolis Monte Carlo relies on the Markov chain's random microstructure state. In addition to commonly studied variables, the proportion of chemical composition was demonstrated to substantially impact fatigue strength if fatigue lifetime in crack propagation did not prevail due to high threshold internal notches. The study utilizes an algorithm typically used for quantum mechanics to solve the complicated multifactorial fatigue problem. The inputs and outputs are modified by fitting the microstructural heterogeneities into the Metropolis Monte Carlo algorithm. The main advantage here is applying a general-purpose nonphenomenological model that can be applied to multiple influencing factors without high numerical penalty.

KEYWORDS

additive manufacturing, machine learning, Markov chain, Monte Carlo simulation, reinforcement learning, very high cycle fatigue

1 | INTRODUCTION

Machine learning (ML), deep learning, and artificial intelligence are all fields that are quickly expanding in importance. There is a possibility that these new technologies will have a transformative effect on materials, processes, and structures engineering (MPSE). It is argued that an immediate need exists to broaden the usage of these new tools across MPSEs.[1,2] This stems from the advantage of this class of models which is the ability to study complex relations without high numerical or experimental efforts. Numerous statistical and ML techniques can theoretically be used for prediction and inference.

In comparison, ML focuses on prediction by employing general-purpose learning algorithms to find patterns in data that are often thick and difficult to handle.[3,4] For example, aircraft structural health monitoring (SHM) is a technique in which sensors evaluate a structure's present condition of aging and degradation. Aerospace industries utilize artificial intelligence as a novel component of SHM and a knowledge discovery

technique based on temporal dilation in real-time and genetic programming. It highlights that engineers attempting to use artificial intelligence for aircraft SHM are challenged by various industry-specific problems.[5,6] In this context, SHM analysis was performed using an auto-associative neural network (AANN), and radial basis function (RBF) network models were utilized to analyze nonlinear neural networks.[7] However, the selection of features for this network was not straightforward, and thus, the outcome depended on how clever the selection was. In contrast, the model presented here will treat all features equally with an arbitrary number from the beginning, and the algorithm deduces the degree of relevance on its own.

1.1 | ML in materials processing and engineering

Another field of application is additive manufacturing (AM). Compared with traditional subtractive manufacturing, additive AM garners growing interest from academia and industry because of its distinct benefits. Traditional numerical and analytical models are difficult to establish a process-structure–property-performance connection for AM. ML is a reliable approach for pattern identification, especially when it does not require constructing and solving physical models.[8,9] Therefore, the model presented in the next section will focus on bypassing the complex physical phenomena involved in the fatigue damage process for numerical efficiency by focusing on a nonphysical general-purpose algorithm and its formulation. In addition, the density functional theory (DFT) community has been using ML to examine combinations of elements and crystal structures to discover new materials.[10,11] However, in the approach used by Allam et al.,[11] the underlying relationships between inputs and outputs had to be found first between inputs and outputs using DFT and then the neural network was only applied to assess the importance of each parameter. In the Metropolis algorithm presented here, the employment of the preparation phase by numerical techniques will not be necessary. Only the marginal distributions of the considered features are needed to be available at the beginning so the Bayesian part of the algorithm can function properly. In the comprehensive review of Johnson et al.,[10] it was clear that there is an overreliance on neural networks. It is mostly supervised learning in AM with nearly no reinforcement learning (RL) applied to this field. The authors would like to then fill and exploit this knowledge for the interests of the AM and fatigue communities.

1.2 | ML in fatigue

Some researchers also used ML to detect fatigue cracks. Fatigue crack detection has garnered considerable attention due to its impact on everyday safety.[12] It is difficult to minutely test megastructures (such as bridges and buildings) with vibration or ultrasonic sensors; therefore, vision-based fatigue crack detection is recommended[13] in research. It suggests a method for detecting fatigue fracture development based on ML that blends computer vision. Computer vision is utilized to generate data in model,[14] while ML is used to predict fractures based on historical precedents. The experimental findings demonstrate the efficacy of the approach. However, owing to the crack dataset's fragility, certain deviations occur.[15] However, this work did not consider microstructural heterogeneities and scatter bands were confining experimental results strong enough. Therefore, these points will be stressed in the presented model, especially in the very high cycle fatigue regime.

Furthermore, investigating stages II and III of crack development rate built a unique and unified ML-based technique. Naturally, predicting the conditions of the development of fatigue cracks is critical when estimating the residual life of machine components or doing failure analysis.[16] Microstructural heterogeneity was not considered in the same context, and large datasets were needed to achieve reasonable accuracy. However, we introduce an indirect inference about fatigue strength and scatter based on marginal distributions of microstructural heterogeneities.

Mean stress is key in fatigue design, especially in high cycle service.[17] The issue arises from the Fourier transformation combining all cycle-by-cycle mean stress effects into a single zero frequency content. Nonlinear generalization was possible in artificial neural networks (ANNs).[18,19] Although good accuracy was reached in these attempts, there was no consideration of microstructural heterogeneity, especially in the very high cycle fatigue (VHCF) regime. A neuro-fuzzy-based ML approach was used to estimate the high cycle fatigue (HCF) life of laser powder bed fusion (L-PBF) stainless steel 316 L by entering parameters for processing/postprocessing and static tensile properties. However, due to the heterogeneity of the provided data, straight application of the model yielded a range of predictable inaccuracies.[20,21] Processing and postprocessing parameters were considered in the latter model. However, the model was not microstructure sensitive and did not consider the VHCF regime. The total fretting fatigue life of Al4%Cu alloy was predicted using contact size, peak pressure, remote specimen tension, and tangential force ratio. About 90% of the data was used to train and test an

ANN.[22] The neural network was extremely good at discriminating between low-life and run-out outcomes. One main outcome was that the Bayesian regularization training method outperformed the Levenberg–Marquardt approach in terms of performance.[23] The influence of corrosion was studied, but there was no correlation between fatigue strength and microstructural parameters. This we aim to redeem with this contribution.

1.3 | Interdisciplinary application of ML

In another study, uncertainties arising from geometry, material, and models were extensively quantified using data from measurements and tests to estimate the life of fatigue crack growth (FCG) on turbine discs. The Gaussian process regression technique was introduced to describe the accuracy and computational efficiency of high model accuracy measurements.[24] However, the procedure required finite element analysis as an input to the Bayesian approach. A probabilistic fatigue S–N curve was suggested to estimate a probabilistic physics-guided neural network (PPNN). The model addressed limitations inherent in existing parametric regression and traditional ML techniques for interpreting fatigue data. Compared with explicit regression-type models, the PPNN was more adaptable and did not impose constraints on function types under various stress levels, mean stresses, or other variables.[25] For this approach, a correlation to microstructural heterogeneity was not established. In Zhan and Li,[26] the fatigue damage characteristics of AM aerospace alloys were investigated using a novel technique combining physical damage and artificial intelligence models. The continuum damage mechanics (CDM) theory was efficiently integrated with ML models. Theoretical CDM models with AM process-induced effects were provided, followed by numerical computations of fatigue lifetimes. Over 500 data sets were gathered and used to train ML models. However, for an arbitrary parameter selection, we would like to avoid here in the current study a nontrivial CDM calculation that is required as an input for that algorithm. The microstructural heterogeneity means that the domains of the microstructure are having diversity in density and type of lattice defects, crystallographic orientation and mesoscale defect types, and morphology; thus, they give rise to localized plastic deformation under relatively low fatigue loading levels and cause ultimate failure with a significant scatter in the expected strength.

A ML technique for direct analysis was used to estimate the fatigue life of metallic materials with oblique hyperbola and bilinear mode S–N curves. A Bayesian optimization-based inverse analysis was used to evaluate the fatigue limit of the materials (AISI 316, 4140, and CA6NM series). Except in a few situations with considerable variations, the projected fatigue limits matched or slightly undershot the actual values.[27] In contrast, we aim for enhanced accuracy and microstructural mapping on fatigue strength. Experimental data and ML validated a theoretical framework for the life prediction of AM alloys under cyclic loadings.

Further work demonstrated a computational technique from two angles: numerical implementation and random forest model building without being sensitive to microstructure.[28] A hybrid method combined data-driven and model-based techniques for calculating bearings' residual useful life (RUL). Relevance vector machines (RVMs) were used to pick a small number of meaningful basis functions, referred to as relevant vectors (RVs). The RVM was used to identify the most important basic functions on the smoothed data, which were then fitted to the deterioration model and extrapolated to failure.[29] Unlike traditional empirical damage models, a model which could automatically discover the optimal mapping relationship from training data used extensive experimental data from nine materials to calibrate itself implicitly. In predicting the remaining life, the proposed model outperformed conventional models.[30] We observed a reliance on extensive experimental data without a strong correlation to microstructure.

1.4 | Comparative aspects of the current study

The flaws sustained during L-PBF are responsible for the manufactured metallic components' poor fatigue performance and significant lifetime scatter.[31] The support vector machine (SVM) model demonstrates a high capacity for addressing these influences of effects outside microstructure and powder characteristics for Ti-6Al-4V.[32] Miniature specimen tests, statistical methods, and ML techniques were used to study Inconel 718 fatigue life scattering and prediction. It was evident that the size and/or the number of pores in the specimens degraded the fatigue life[33]; therefore, we would like to extend the capability of these models by using RL and including further arbitrary features. In the same context, the research looked at the elements influencing fatigue strength utilizing a hybrid approach combining XGBoost[34] and LightGBM.[35] A grey wolf algorithm optimizes the model hyperparameters.[36] Shapley additive explanations (SHAP) are developed to explain ML model predictions of fatigue strength.[37] According to the results, the SHAP approach showed much potential for evaluating fatigue strength indicators. Therefore, rationalized design parts,

selecting materials, and formulating cold and heat resistant materials were deemed possible using the technique.[38] Micromechanical models accurately represented material behavior and its relationship to thermal history from the early stages of computational materials science.[39] However, when out-of-range data were used to train ML models, projected grain sizes varied significantly from reference values. Supervised learning (SL) had a weaker capacity to generalize to previously unknown data than random forest regression (RFR) when it came to damage evolution prediction.[40] In Zhan and Li,[41] a framework was created for data-driven analysis of AM stainless steel (SS) 316L fatigue life prediction using CDM. Three common ML models are effectively trained using a CDM-generated database. Additional comparisons between anticipated and published experimental data were attempted to validate the suggested platform. The microstructural influence was indirectly included in the algorithm through the CDM approach, which we would like to change here by directly considering these arbitrary parameters.

The structural information of a shackle used to efficiently connect components to the hoist was gathered using two strain sensors of a dual system. The signal was processed and classified as normal or abnormal. The decision boundary was determined using logistic regression ML. The results show that failure may be identified before fracture appears and that maintenance could be delayed.[42] In Sysyn et al.,[43] images of the frog rolling surface and magnetic particle inspection data were used in the ML investigation. The scans were preprocessed using image processing algorithms to identify characteristics similar to surface cracks. Surface fractures may not be seen in raw images.[44] These fracture properties and their combinations properly depict surface fatigue.[43] In practice, the time-consuming magnetic particle imaging (MPI) inspection approach does not apply to low-automation railway infrastructure.[45] A state-of-the-art object detector was introduced, capable of training models from scratch. The models developed from sparse data demonstrated a fair aptitude for identifying fatigue fracture start locations.[46] Increasing the amount of the training dataset could enhance the model's accuracy.[47] Increased epochs could result in an enhanced capacity to identify subtle characteristics.[46]

A semi-empirical S–N fatigue model was developed based on uniaxial and multiaxial fatigue investigations. It accounted for both material anisotropy and complex stress states and has an average inaccuracy of 20.70%. Six ML models were used to estimate fatigue life, and the deep neural network was found to be the most accurate, with an average accuracy of 14.30%.[48] However, the model was applied for rubber and composites, and metallic materials were not included. The collection of bridge-specific traffic loading data via the weigh-in-motion (WIM) system provided an opportunity to remedy the issue of unexpected failures in highly congested bridges.[49] Daily fatigue damage may be calculated using traffic loading data in conjunction with finite element analysis. To establish regression models between daily damage and collected traffic loading characteristics, a SVM was used, which was validated by predicting the fatigue life of a suspension bridge hanger.[50] An approach for forecasting fatigue damage patterns inside the steel catenary risers was presented in addition to numerical simulation and a random sampling technique. The suggested technique could correctly and efficiently calculate the fatigue life of a sample riser.[51]

1.5 | RL brought to the fatigue community

This study applies a RL ML algorithm based on Bayesian inferential statistics using the Metropolis Monte Carlo algorithm to estimate the posterior distributions. The case is on additively manufactured AlSi12 alloy to identify influence of microstructure, remnant porosity, chemical composition, and powder particle size. Barto and Duff explain that RL is more efficient than other types of learned techniques capable of obtaining the same outcomes with link to Monte Carlo techniques.[52] We have found in the review in this section that RL has not been used to address the fatigue problem. However, in quantum mechanics, the phases of classical spin models were classified using improved estimators by ML applied to the quantum Monte Carlo simulation using the loop algorithm.[53] Monte Carlo or deep learning has been claimed to be used to solve extremely high-dimensional partial differential equations (PDEs), using concepts from either nonlinear or linear algebra (multilevel). They are potentially curse-free for various applications and be so for several nonlinear Monte Carlo techniques for nonlinear parabolic PDEs.[54] Foreman et al.[55] generalized the Hamiltonian Monte Carlo approach using a stack of deep learning neural network layers and assessed its ability to sample from various topologies in a two-dimensional lattice gauge theory. Based on these previous precedents in the literature, we would like to introduce a RL technique based on the Metropolis Monte Carlo algorithm to study the influence of structural heterogeneities on VHCF strength in AM. We observe in the literature that RL and the Metropolis Monte Carlo algorithm have been used to solve complicated physical problems optimally. However, the fatigue and AM communities did not utilize any of the power of these algorithms until now. Moreover,

microstructure-sensitive simulations have a very high numerical penalty, and a limited set of heterogeneous microstructural parameters can be included in the analysis. Therefore, we introduce here a general-purpose non-phenomenological RL algorithm that is applicable until the high cycle fatigue regime can handle an arbitrary number of microstructural parameters.

2 | MATERIALS AND METHODS

2.1 | Training data

This study's ML technique uses a decision tree to guide data via a network representing fatigue-related factors such as the start of macroscopic failure and threshold stress. Simultaneously, a family of extreme value gamma distributions is employed to prevent undershooting or overshooting the target values. The Weibull distribution presented here is based on the gamma function[56,57]

$$Q(N,\Delta\sigma)=1-exp\left\{-\left[\frac{(logN-B)(g(\Delta\sigma)-C)-\lambda}{\delta}\right]^{\beta}\right\} \quad (1)$$

where N is the number of cycles, $\Delta\sigma$ is the applied stress range, β is the shape parameter, δ is the scale parameter, λ is the location parameter, B is the fatigue lifetime threshold, and C is the fatigue strength threshold. The maximum likelihood method is used for initial parameter estimation according to Walpole and co-workers in addition to Castilo and co-workers.[57,58]

2.1.1 | Manufacturing and initial characterization

The laser beam melting system SLM 250HL was used to fabricate all specimens in this investigation from AlSi12 powder. The device is equipped with a 400 W fiber laser and can reach temperatures up to 200°C in the deposition platform to reduce cooling rates. Argon was employed as an inert gas in the construction chamber. Laser scanning was performed using a technique known as checkerboard scanning. The details of laser scanning energy density can be found in previous studies.[59–61] Mechanical testing specimens were stress-relieved (SR) for 2 h at 240°C, followed by cooling in the oven; see Table 1. Additionally, batch B was platform-heated (PH) up to 200°C such that the cooling rate was significantly reduced according to Siddique et al.[62] which led to a reduction in remnant porosity and improvement of fatigue strength, especially in the VHCF regime according to Siddique et al.[60] The influence of PH was less pronounced in AlSi10Mg, according to Awd et al.[63]

2.1.2 | Microstructural heterogeneity

The microstructure of the tracks was investigated by embedding cross-sections in the *XY* plane (parallel to the building platform) and *Z* plane (perpendicular to the building platform). Grit paper ranging from 320 to 4000 was used for grinding, which was lubricated with water. Polishing was then performed down to a diamond suspension of 1 μm, and the ultimate finish was achieved using a chemical polishing solution, including oxide suspension. A Tescan Mira XMU scanning electron microscope (SEM) was utilized to get high-magnification images of Si dendrites. In advance, specimens were etched using a solution of 10% NaOH and 10% H2O2 in distilled water at a temperature of 60°C. The chemical composition was quantified using an energy dispersive X-ray detector of type EDAX operating at a voltage of 20 kV and beam intensity of 15 A. The chemical composition of powder was characterized in the fresh and used states. Figure 1 depicts the microstructural morphology of the investigated batches based on the thermal history. Comparing the microstructures of batches A and B shows that batch A has a very thin cellular dendritic microstructure with a pronounced texture. That can be detected from bottom to top in the building direction (*Z*-axis). The reduced cooling rate facilitated Si particle segregation at the grain boundary. Si accumulation at grain boundaries led to the production of dendrites with a greater thickness which was also asserted by Prashanth et al.[64] From LCF to the VHCF regime, this change has yet to have a major influence on the link between quasi-static and cyclic characteristics. The load-bearing *Z*-direction microstructure in batch B is almost equiaxed compared with the microstructure in the *Z*-direction in batch A.

TABLE 1 Investigated material configurations based on the thermal history

Batch	Alloy	Platform heating (PH)	Stress relief (SR)
A	AlSi12	–	240°C
B	AlSi12	200°C	240°C

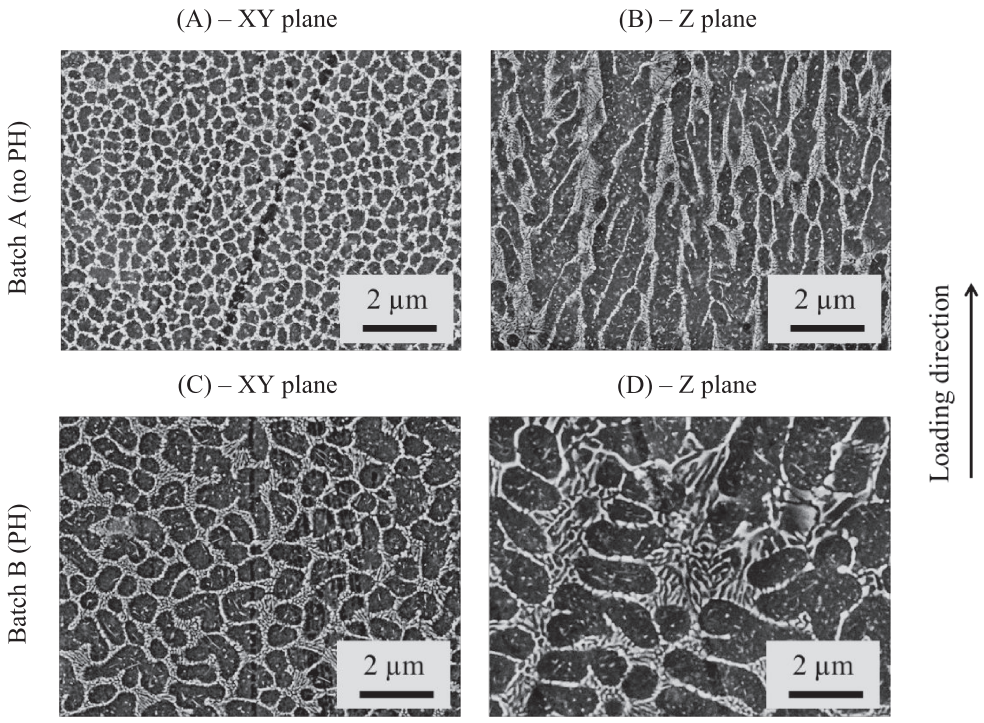

FIGURE 1 Influence of thermal history of Table 1 on microstructural morphology: (A) batch A—*XY* plane; (B) batch A—*Z* plane; (c) batch B—*XY* plane, adapted from Siddique et al.[58]; (D) batch B–*Z* plane; loading direction concerning the microstructure in the *Z* plane in (B and D)

Numerous investigations have shown that selective laser melted Al-Si alloys are prone to residual porosity.[62,65] Certain researchers investigated porosity using two-dimensional metallographic methods.[66,67] Others used three-dimensional methods such as X-ray micro-computed tomography (µ-CT) to determine flaws' shape, size, and position in three-dimensional space.[68–70] The Varian® PaxScan 1313DX detector, based on amorphous silicon, is equipped to capture the projected pictures. The effective detector size is 13 × 13 cm^2, with a pixel count of 1024 × 1024 pixels and a pixel pitch of 127 µm. Nikon's X TH 160 system has a cesium iodide (CsI) scintillator conversion screen with a 40–160 kV energy range. Reconstruction of a two-dimensional picture stack may be used to create a three-dimensional representation of the scanned specimen using VGStudio Max 2.2. A fatigue specimen is coaxially fastened to the table in this investigation, allowing X-rays to pass through each projection of the specimen. The projected two-dimensional gray value distribution exhibits flaws and inhomogeneities distributions. Volumetric three-dimensional distributions of defects can be found in.[71] Figure 2 reports the shape parameter β and scale parameter δ for the probability distribution of the pore diameter inside batches A and B, according to Maltamo et al.[72] Table 1 reported the same statistical parameters for the dendritic width in the *XY* plane and in the *Z* plane. The powder parameters are the particle size and the weight

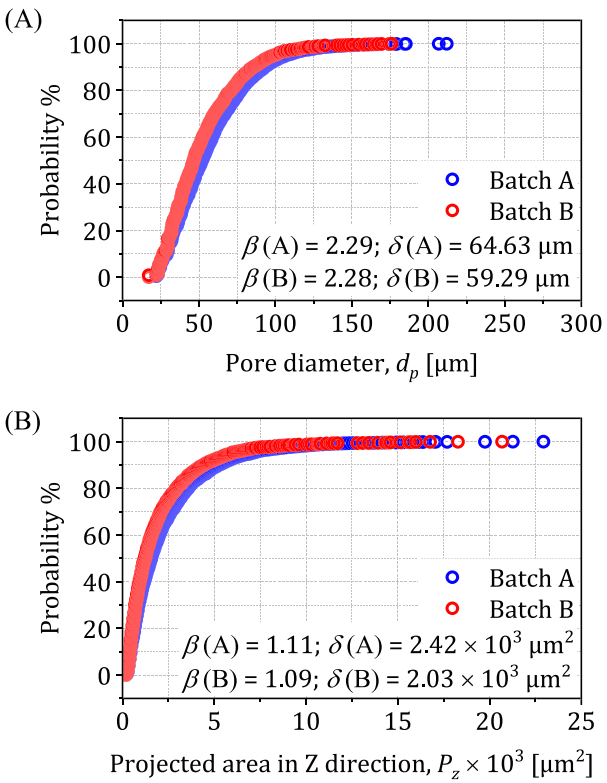

FIGURE 2 Probability distributions of defect characteristics as detected by µ-CT for batches A (no PH) and B (PH): (A) pore diameter; (B) projected area in the *Z*-direction—Input of the model [Colour figure can be viewed at wileyonlinelibrary.com]

percentage of the aluminum element in the new and used powder.

2.1.3 | Influence of heterogeneities on cyclic deformation behavior

The following fatigue tests were conducted during the training and validation phases of the model application. Tensile tests were performed on the specimens using an extensometer with a gauge length of 10 mm on an Instron 3369 machine equipped with a load cell of 50 kN. The tensile testing results can be found in Awd et al.[71] All specimens were subjected to two distinct kinds of stress-controlled fatigue testing. The first is the load increase test (LIT), which involves subjecting the specimen to an increasing stress amplitude as a function of time through a constant ramp. Thus, the cyclic response of a material to a broad range of stresses can be monitored, and cyclic fully reversed critical fatigue stress amplitudes may be determined. Following the material's response to the stress ramp may be utilized to identify crucial stress amplitudes at which new mechanisms of fatigue damage become active in the transition from HCF to low cycle fatigue (LCF). The second kind is a constant-stress amplitude fatigue test performed at predetermined levels following the damage response seen during the LIT. The approach incorporating both types is utilized as a high-throughput method for determining the fatigue strength of materials and filtering out unsuitable load applications. The LIT and constant amplitude tests (CAT) were performed on a servohydraulic Instron 8872 system equipped with a 10 kN load cell. The specimen geometry can be found in Awd et al.[71] In Figure 3, the total strain amplitude evolution separates the LCF regime from the HCF regime at 130 MPa of stress amplitude. Therefore,

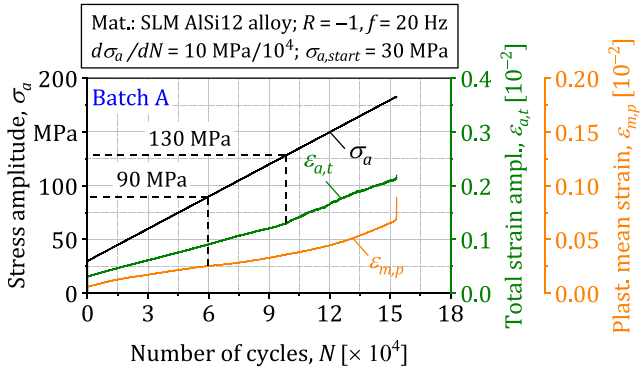

FIGURE 3 Total strain amplitude build-up and mean plastic strain accumulation in the load increase test indicating critical loading amplitudes in batch A (no PH) [Colour figure can be viewed at wileyonlinelibrary.com]

constant amplitude testing will be done at the levels above and below, focusing on the 120 and 140 MPa levels for the low frequency (20 Hz) testing at the servohydraulic systems. Meanwhile, the plastic mean strain curve has an inflection point at 90 MPa, indicating the transition value of stress amplitude at the late HCF and the beginning of the VHCF regimes for which CAT will be conducted at 20 kHz on the USF-2000A of Shimadzu.

2.1.4 | Influence of heterogeneity on fatigue strength

In the USF-2000A, the actuator generates a 20 kHz longitudinal oscillation (from a piezoelectric element). The booster and horn then amplify the actuation to impart a force on a specimen. Since 20 kHz longitudinal oscillation uses resonance, precise adjustment is essential to ensure that the whole oscillation system (booster, horn, specimen, etc.) is resonating at 20 kHz. Because the booster and horn are pretuned, just making a specimen that resonates at 20 kHz causes the whole oscillation system to resonate at that frequency. Metals' longitudinal vibration causes resonating longitudinal waves as an Eigen natural frequency value. In other terms, it implies that metals are subjected to repetitive stress-loading during this test. The specimen's side amplitude displacement determines the stress value because this system tests inside the elastic limit, where macroscopic displacement (strain) is directly proportional to stress according to Hooke's law. Therefore, in theory, test force cannot be directly measured with a typical load cell. The specimen's side displacement value is determined using linear interpolation from the vibrational calibration procedure. The specimen gets heated repeatedly when subjected to high-frequency loading. As a result, forced air conditioning and interrupted driving help cool it down as close as possible to the starting temperature of the test. Interrupted driving is a cycle in which ultrasonic waves are produced for a brief period and then stopped for a period. The testing setup can be found in detail in previous studies.[73,74] Figure 4 depicts the S–N curves of batches A and B for both high- and low-frequency tests. We can attend a reciprocation of fatigue strength at the end of the HCF range. Batch A had a greater fatigue strength in the early HCF range than batch B. In Figure 1, batch A had a much finer microstructure than batch B. Due to the increased density of grains in a given specific volume, a saturation of single grains with strain occurs more rapidly. The load is redistributed when the load axis in columnar grains is perpendicular to the grain axes. Under conditions of increasing stress amplitude, the net stress from each grain is partly or completely canceled off by

the net stress in nearby grains.[71,75] Hybrid construction of additively manufactured and wrought aluminum alloys could achieve similar VHCF strength to batch B.[76] Testing at 20 kHz leads to an extremely high local strain rate, significantly affecting the grains' critical resolved shear stress. Since the early phases of fatigue damage rely on dislocation slip, the testing at a high strain rate influences the number of cycles to failure. Such complicated physical damage mechanisms require high penalty phenomenological modeling to account for and study the corresponding effect. Therefore, the model introduced here is a data-driven approach that handles data irrespective of the phenomenological evolution. The advantage is the additional handling of heterogenous fatigue data produced at extremely different frequencies.

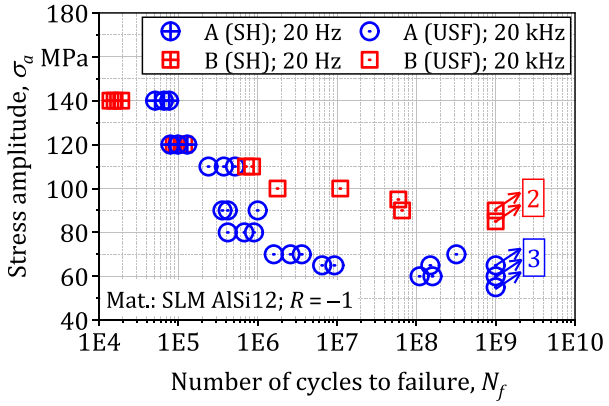

FIGURE 4 Experimental S-N data of batches A (no PH) and B (PH) at frequencies of 20 Hz and 20 kHz according to previous studies[60,61,73] [Colour figure can be viewed at wileyonlinelibrary.com]

Figure 5 shows a specimen heavily infested with defects tested at 120 MPa of stress amplitude. Although the specimen had this significant number of defects, the failure did not start from the defect with the largest size or asymmetric morphology, as shown in Figure 5A. Bending stresses can increase the stress field's intensity near the specimen's surface. They were accounted for by using a self-aligning jig before the beginning of the test at 20 Hz. In the 20 kHz tests, the specimens were designed to have an eigenfrequency mode in the uniaxial direction only. Thus, bending stresses were also avoided at USF-2000A. However, a cluster of pores in the immediate subsurface of the specimen initiated the failure, a phenomenon repeatedly found in the literature for Al-Si alloys.[62,77] Figure 5B shows a short crack propagation zone with small-scale yielding and relatively smooth crack surfaces. In (D), (E) zone 1, and (F), secondary failure initiating zones were observed; however, they were retarded by the microstructure and were not activated until the final fracture of the specimen. In (C) and (E) zone 2, we observed the disintegration of melt pool boundaries due to local spherodization of the microstructure and strain localization. This results from excessive defects in the melt pool overlap zones.

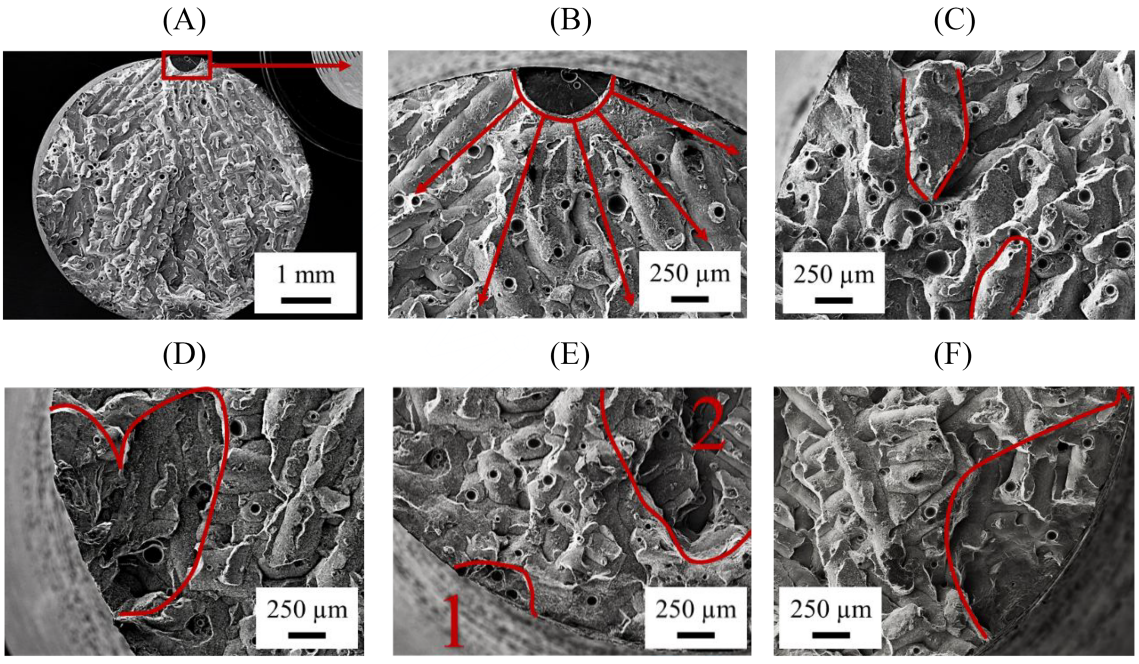

FIGURE 5 Failure initiation defects morphology in batch A (no PH) at stress amplitude of 120 MPa at 20 Hz of frequency: (A) overview of fracture surface; (B) overview of failure responsible defect; (C) highlights of specific melt pool morphologies; (D) clustering of defects at the surface and inside the volume; (F) secondary crack initiation [Colour figure can be viewed at wileyonlinelibrary.com]

2.2 | Theory and calculation

Monte Carlo algorithms and procedures can contribute to the development of posterior estimation of the fatigue conjugate $f(N,\Delta\sigma)$ which is a simulation-based inference.[78] In a purely statistical setting, computational problems arise at the level of probabilistic modeling of the fatigue strength inferred rather than at the statistical inference from fatigue-related influences.[79] As an example, in a specific scenario of a fatigue problem, a comprehensive description of the causes leading to a certain fatigue damage scenario might result in a complicated formulation that is too complex to be represented by a parametric representation and impractical to solve with available numerical tools.[57] A prohibitive numerical example that can be recalled here is solving a representative volume element (RVE) under laboratory fatigue conditions. It contains a typical defect morphology of AM processes using the crystal plasticity finite element method (CPFEM) until the number of cycles to failure is reached. This is the technical problem we would like to circumvent here by presenting this data-driven approach.

2.2.1 | Monte Carlo approximation

Formulation of procedure based on microstructure

Our parameter of interest is the fatigue conjugate $f(N,\Delta\sigma)$, and we let $(N,\Delta\sigma)_1,\ldots,(N,\Delta\sigma)_n$ be the numerical conjugates of a sample from a distribution of stress-life conjugates $p\left((N,\Delta\sigma)_1,\ldots,(N,\Delta\sigma)_n\,|\,M\right)$ based on experimental data, for instance, given a certain state of microstructural sample M. Suppose we are to sample some number S of independent, random microstructures M-values from the posterior distribution of the microstructure given conjugates of corresponding fatigue strength and stress ranges $p\left(M|(N,\Delta\sigma)_1,\ldots,(N,\Delta\sigma)_n\right)$ such that[78,80]

$$M^{(1)},\ldots,M^{(S)}\sim i.i.d\ p\left(M|(N,\Delta\sigma)_1,\ldots,(N,\Delta\sigma)_n\right) \tag{2}$$

i.i.d. stands for independent and ideally distributed random variable. Then the empirical (based on laboratory findings) distribution of the microstructural samples $\left\{M^{(1)},\ldots,M^{(S)}\right\}$ would approximate conditional probabilities given the stress-life conjugates $p\left(M|(N,\Delta\sigma)_1,\ldots,(N,\Delta\sigma)_n\right)$, with the approximation improving with increasing the sample size S. The empirical distribution, when large enough, of microstructural samples $\left\{M^{(1)},\ldots,M^{(S)}\right\}$ is known as a Monte Carlo approximation to $p\left(M|(N,\Delta\sigma)_1,\ldots,(N,\Delta\sigma)_n\right)$. In this study, this procedure will be programmed on Matlab after being detailed in the next lines. Additionally, let $g(\theta)$ be the marginal distribution of the microstructure which means the probability distribution of the sample subset. The law of large numbers says that if $M^{(1)},\ldots,M^{(S)}$ are *i.i.d.* samples from the microstructure given the stress-life conjugates $p\left(M|(N,\Delta\sigma)_1,\ldots,(N,\Delta\sigma)_n\right)$, then[80,81]

$$\begin{aligned}\frac{1}{S}\sum_{s=1}^{S}g\left(M^{(s)}\right)&\rightarrow E\left[g(M)|(N,\Delta\sigma)_1,\ldots,(N,\Delta\sigma)_n\right]\\&=\int g(M)p\left(M|(N,\Delta\sigma)_1,\ldots,(N,\Delta\sigma)_n\right)dM\ as\ S\rightarrow\infty\end{aligned} \tag{3}$$

This suggests that as the sample gets larger, preferably and theoretically approaching infinity $S\rightarrow\infty$

- The mean value of the microstructural sample is $\overline{M}=\frac{1}{S}\cdot\sum_{s=1}^{S}M^{(s)}\rightarrow E\left[M|(N,\Delta\sigma)_1,\ldots,(N,\Delta\sigma)_n\right]$, where E stands for the estimate.
- Correspondingly, the estimate of variance from the stress-life conjugates would be

$$\frac{1}{(S-1)}\cdot\sum_{s=1}^{S}\left(M^{(s)}-\overline{M}\right)^2\rightarrow Var\left[M|(N,\Delta\sigma)_1,\ldots,(N,\Delta\sigma)_2\right].$$

Such that the probability that our sample is less than an actual value c can be estimated by the stress-life conjugate

$$\#\frac{M(s)\le m}{S}\rightarrow P\left(M\le m|(N,\Delta\sigma)_1,\ldots,(N,\Delta\sigma)_n\right).$$

This is given that laboratory data enable us to estimate the empirical distribution of microstructure using the stress-life conjugate

$$\left\{M^{(1)},\ldots,M^{(S)}\right\}\rightarrow p\left(M|(N,\Delta\sigma)_1,\ldots,(N,\Delta\sigma)_n\right).$$

The median value[56] of the microstructural sample is $\left\{M^{(1)},\ldots,M^{(S)}\right\}\rightarrow M_{1/2}$.

The $n_{th}-$ percentile of $\left\{M^{(1)},\ldots,M^{(S)}\right\}\rightarrow M_n$.

2.2.2 | Identification of unique statistical fatigue parameters

Just about any statistical feature of the posterior distribution of a fatigue-related influence, we may be interested

and can be approximated arbitrarily exactly with a large enough Monte Carlo sample of the parameter of interest. In this study, we would like to utilize this concept in the fatigue problem since it is not used before and use it to investigate fatigue and structure correlations which are rarely discussed in the literature according to the introduction of this article. Hence, the predictive distribution of a random microstructural $M(S)$ is the probability distribution of M such that[80]

- known parameters have been conditioned on. In different words, the study is designed such that the parameter of interest becomes dependent on the observed parameter. The parameters of thermal history are based on, for example, platform heating; see Table 1 or in situ thermal treatment such as in previous studies.[82,83]
- unknown parameters have been integrated out, such as stress and fatigue lifetime conjugates $f(N, \Delta\sigma)$; Figure 4. It means that there is enough data in the S–N curve to define the relationship between loading and the number of cycles to failure such that the statistical dependency of a lifetime on applied load is ruled out.

We let $\widetilde{N}$ be the fatigue lifetime sampled from a batch manufactured with specific thermal history and powder parameters. If we knew the true mean failure rate θ of this specimen, we might describe our uncertainty about $\widetilde{N}$ with a $gamma\left(\widetilde{N}_f\right)$ distribution[57,72]

$$\begin{aligned}\text{Sampling distribution } P\left(\widetilde{N}=\widetilde{N}_f|\theta\right) &= p\left(\widetilde{N}_f|\theta\right)\\ &= \theta\cdot exp\left[-\left(\left(\widetilde{N}_f-\lambda\right)/\delta\right)^{\beta}\right]\end{aligned}$$

where the failure rate θ is defined as $\theta = \beta/\delta\left(\left(\widetilde{N}_f\ -\lambda\right)/\delta\right)^{(\beta-1).}$ where $\widetilde{N}_f$ is an approximation of the number of cycles to failure. β is the shape parameter, δ is the scale parameter, and λ is the location parameter. It is not possible to make predictions from this model, however, because we do not know θ yet. If we did not have any fatigue data from the population, our predictive distribution would be obtained by integrating out θ to estimate the predictive distribution: $P\left(\widetilde{N}=\widetilde{N}_f\right) = \int p\left(\widetilde{N}_f|\theta\right)p(\theta)\,d\theta$. Such a distribution can be useful in evaluating if the failure rate prior distribution for θ represents prior beliefs (empirical fatigue data) for observable fatigue lifetime data $\widetilde{N}$ in the laboratory; after we have observed a sample $N_1, ..., N_n$ from the batch population, the relevant fatigue lifetime predictive distribution for a yet to infer or estimate stress-lifetime conjugates $f(N, \Delta\sigma)$ conjugate reads

$$\begin{aligned}&P\left(\widetilde{N}=\widetilde{N}_f|N_1=N_{f1},...,N_n=N_{fn}\right)\\ &= \int p\left(\widetilde{N}_f|\theta,N_{f1},...,N_{fn}\right)p\left(\theta|N_{f1},...,N_{fn}\right)\,d\theta\\ &= \int p\left(\widetilde{N}_f|\theta\right)p\left(\theta|N_{f1},...,N_{fn}\right)\,d\theta\end{aligned} \tag{4}$$

This is called a posterior predictive (estimated) distribution of stress-fatigue lifetime conjugates $f(N, \Delta\sigma)$ because it conditions the fatigue failure-related influence dataset on the failure rate induced by certain parameters of interest such as microstructure. In many fatigue lifetime prediction situations, we will be able to extract a sample from $p\left(\theta|N_{f1},...,N_{fn}\right)$ and $p\left(N_f|\theta\right)$, but $p\left(\widetilde{N}_f|N_{f1},...,N_{fn}\right)$ will not be practical to sample from directly since a large enough amount of fatigue tests is economically prohibitive. We can indirectly sample from the posterior predictive distribution using a Monte Carlo procedure in this situation. Since $p\left(\widetilde{N}_f|N_{f1},...,N_{fn}\right) = \int p\left(\widetilde{N}_f|\theta\right)p(\theta|N_{f1},...,N_{fn})\,d\theta$, we see that $p\left(\widetilde{N}_f|N_f1,...,N_fn\right)$ is the posterior expectation of $p\left(\widetilde{N}_f|\theta\right)$.[84,85] To obtain the posterior predictive probability that $\widetilde{N}$ is equal to some specific value $\widetilde{N}_f$, we could just apply the Monte Carlo method: Sample $\theta^{(1)},...,\theta^{(S)} \sim i.i.d.\ p\left(\theta|N_{f1},...,N_{fn}\right)$ and then approximate $p\left(\widetilde{N}_f|\theta,N_{f1},...,N_{fn}\right)$ with $\sum_{s=1}^{S}p\left(\widetilde{N}_f|\theta^{(s)}\right)/S$. This procedure will work well if $p\left(N_f|\theta\right)$ is discrete, and we are interested in quantities that are easily computed from $p\left(N_f|\theta\right)$. However, it will generally be useful to have a set of samples of $\widetilde{N}$ from its posterior predictive distribution. Obtaining these samples is a simple process that may be accomplished by considering the failure rate: $\theta \approx$ the microstructure: M (for generalization to arbitrary parameters), as follows:

$$\text{sample}\,\theta^{(1)} \sim p(\theta|N_{f1},...,N_{fn}),\ \text{sample}\,\widetilde{N}_f^{(1)} \sim p\left(\widetilde{N}_f|\theta^{(1)}\right)$$

$$\text{sample}\,\theta^{(2)} \sim p(\theta|N_{f1},...,N_{fn}), \quad \text{sample}\,\widetilde{N}_f^{(2)} \sim p\left(\widetilde{N}_f|\theta^{(2)}\right)$$

...

$$\text{sample}\,\theta^{(S)} \sim p(\theta|N_{f1},...,N_{fn}), \ \text{sample}\,\widetilde{N}_f^{(S)} \sim p\left(\widetilde{N}_f|\theta^{(S)}\right)$$

In other words, the sample represents several experimental fatigue tests corresponding to a microstructural condition. The sequence $\left\{\left(\theta,\widetilde{N}_f\right)^{(1)},...,\left(\theta,\widetilde{N}_f\right)^{(S)}\right\}$ constitutes S independent samples based on microstructure from the joint posterior distribution of $\left(\theta,\widetilde{N}_f\right)$, and the sequence $\left\{\widetilde{N}_f^{(1)},...,\widetilde{N}_f^{(S)}\right\}$ constitutes S independent samples from the marginal posterior distribution of $\widetilde{N}$, which is the posterior predictive distribution.

2.2.3 | Markov chains of microstructural heterogeneities

Let us suppose we have a random transition of fatigue damage states $(\Psi_n)_{n\geq 0}$ in a Bernoulli-like random walk (fatigue damage state progression) that initializes $\Psi_0 = 0$ assuming a damage-free fatigue specimen at the start of a fatigue test[86]

$$\Psi_n = \sum_{k=1}^{n} \psi_k = \psi_1 + \cdots + \psi_n, n \geq 1, \tag{5}$$

where the random unknown damage increments $(\psi_k)_{k\geq 1}$ as a fatigue test progresses, critical damage shifts in a nondeterministic physical manner $\{0,+1\}-$ fatigue indicator parameter, where 0 is a damage-free state, and 1 is a completely damaged state. This resembles a discrete-lifetime stochastic process $(N_n)_{n\in\mathbb{N}}$ in the space of $(\mathbb{N},\Delta\boldsymbol{\sigma})$ which satisfies Equation (4). The $(\mathbb{N},\Delta\boldsymbol{\sigma})$-valued process $(N_n)_{n\in\mathbb{N}}$ is said to be Markov or having the Markov property when $n\geq 1$, the probability distribution of N_{n+1} is determined by the state N_n of the process at time n and does not depend on the previous values of N_k for $k = 0,1,...,n-1$. Thus, when the sequence of fatigue damage states has no memory according to the Markov property. From a different perspective for all $n\geq 1$ (after the start of the fatigue damage process) and all $i_0,i_1,...,i_n,j\in\mathbb{N}$, we have the transition probabilities between damage states presented as follows:

$$\begin{aligned} &P(N_{n+1}=j\,|N_n=i_n,N_{n-1}=i_{n-1},...,N_0=i_0) \\ &=P(N_{n+1}=j|\,N_n=i_n) \end{aligned} \tag{6}$$

especially the satisfaction of the Markov property that there is no memory of the sequence

$$P(N_{n+1}=j\,|N_n=i_n,N_{n-1}=i_{n-1}) = P(N_{n+1}=j|N_n=i_n) \tag{7}$$

For example, the second damage state following the damage-free state and the first state would be

$$P(N_2=j\,|N_1=i_1,N_0=i_0) = P(N_2=j|\,N_1=i_1) \tag{8}$$

Correspondingly, the physically indeterminate progression of a Markov chain is generally based on

$$P_{i,j} := P(N_1=j|N_0=i),\ i,j\in\mathbb{N} \tag{9}$$

which corresponds with the probability $P(N_{n+1}=j|N_n=i)$ which is independent of the location of the current state within the sequence $n\in\mathbb{N}$. In this case, the Markov Chain $(Z_n)_{n\in N}$ is a time homogenous chain since the transition probabilities of fatigue damage states do not depend on time. The data can be comprehensively represented in a transition matrix of the Markov chain[87]

$$\left[P_{i,j}\right]_{i,j\in\mathbb{N}} = \left[P(N_1=j|N_0=i)\right]_{i,j\in\mathbb{N}} \tag{10}$$

The transition matrix contains the entries of a fatigue parameter indicator states that is the most relevant fatigue damage criterion to be sampled from in the Monte Carlo process.

Numerical handling

The treatment starts with sampling from a large transition matrix of fatigue damage parameters, for example, a transition matrix based on microstructure. The entries of the transition matrix must be normalized. A prior distribution is obtained from the structural measurement of the specimens, see Table 2. A local maximum has then to be found to optimize the belief function of fatigue strength. The process is repeated n times to satisfy equation (3). It generates a discrete-time, finite-state, homogeneous Markov chain from a given state transition matrix using discrete-fatigue lifetime, finite-state fatigue damage transitions, and homogeneous Markov chains. It also can associate the states with the various fatigue

TABLE 2 Statistical parameters of the fatigue-related influences for the factors of dendritic width and powder chemical composition and particle size—input of the model

	Dendritic width *XY* plane		Dendritic width *Z* plane	
Statistical parameter	**Batch A**	**Batch B**	**Batch A**	**Batch B**
Shape β	3.26	3.27	2.40	2.27
Scale δ (μm)	0.31	0.41	0.61	0.69
Al wt.%	**Fresh powder**		**Used powder**	
Shape β	27.01		21.53	
Scale δ (wt.%)	88.55		90.85	
Particle diameter	**Fresh powder**		**Used powder**	
Shape β	4.51		2.59	
Scale δ (μm)	25.29		28.97	

damage states within the same matrix. After establishing a dtmc (discrete-time Markov chain) object, we may use the object functions to study the structure and evolution of the Markov chain. Concerning the parameters of interest, as well as to display the Markov chain in various ways, as shown in Section 3.

2.2.4 | RL: The Metropolis–Hastings Monte Carlo algorithm

Formulation

Let us consider a stress-life conjugate $f(N, \Delta\sigma)$ where we have a sampling model on a fatigue indicator parameter $N \sim p(N|\theta)$ and a prior distribution $p(\theta)$. θ stands for a fatigue-related influence and can be replaced by pore diameter d_p or microstructure M or another arbitrary parameter. Although in most fatigue failure cases $p(N|\theta)$ and $p(\theta)$ can be calculated for any set of values of N and θ, $p(\theta|N) = p(\theta)p(N|\theta)/\int p(\theta')p(N|\theta')\,d\theta'$ is often not trivial to calculate due to the integral in the denominator, which represents an accurate knowledge of the dependence between the fatigue indicator parameter θ and the fatigue lifetime N which is numerically or empirically prohibitive to determine. If we were able to sample from the conditional distribution of the fatigue indicator parameter $p(\theta|N)$, then we could generate $\theta^{(1)}, ..., \theta^{(S)} \sim$ *i.i.d.* $p(\theta|N)$ and obtain Monte Carlo approximations to posterior fatigue strength, such that as discussed at the beginning of Section 2.2[80,84]

$$E[g(\theta)|N] \approx \frac{1}{S}\sum_{s=1}^{S} g\left(\theta^{(s)}\right) \tag{11}$$

However, there will be some cases when we cannot sample directly from the conditional fatigue indicator parameter for the distribution $p(\theta|N)$. In terms of approximating the fatigue indicator posterior distribution, the critical issue is not that we have *i.i.d.* samples from $p(\theta|N)$ but alternatively that we can compose a large withdrawal of fatigue-related damage θ-values such as microstructure or porosity, $\{\theta^{(1)}, ..., \theta^{(S)}\}$, whose empirical distribution approximates $p(\theta|N)$. Roughly speaking, for any two different arbitrary fatigue damage cases θ_a and θ_b, the following relation can be established:

$$\frac{\#\{\theta^{(s)}\text{'s in the random experiment/withdrawal} = \theta_a\}}{\#\{\theta^{(s)}\text{'s in the random experiment/withdrawal} = \theta_b\}} \approx p\left(\frac{\theta_a|N)}{p(\theta_b|N)}\right) \tag{12}$$

When we think efficiently about how we compose such a pool of fatigue indicator values, suppose we have the following pool of fatigue indicator parameters $\{\theta^{(1)}, ..., \theta^{(s)}\}$ to which we would like to update it with a recent damage value $\theta^{(s+1)}$ from the transition matrix. Let us suppose we update with a value θ^* which is nearby $\theta^{(s)}$. Should we include θ^* in the pool or not? If its distribution $p(\theta^*|N) > p\left(\theta^{(s)}|N\right)$ which is conditional on the current value, then we want values nearby to θ^*'s in the pool than $\theta^{(s)}$'s. Since $\theta^{(s)}$ is already in the pool, then it seems we should include θ^* as well. On the other hand, if $p(\theta^*|N) < p\left(\theta^{(s)}|N\right)$, then it seems it should not necessarily include θ^* because we are getting further away from the solution; the essence of the reinforced learning algorithm is random sampling and measuring how close we are getting to the solution (Is the current probability higher than the previous probability?). If we get closer to the solution, the sample is accepted; otherwise, rejected; therefore, we reinforce an update on the algorithm if it gets us closer to the solution. So perhaps our decision to include θ^* or not should be based on the relative relation of $p(\theta^*|N)$ to $p\left(\theta^{(s)}|N\right)$. Luckily, this comparison can be

made even if we cannot compute the conditional fatigue indicator parameter $p(\theta|N)$

$$r = \frac{p(\theta^*|N)}{p(\theta^{(s)}|N)} = \frac{p(N|\theta^*)p(\theta^*)}{p(N)} \times \frac{p(N)}{p(N|\theta^{(s)})p(\theta^{(s)})} = \frac{p(N|\theta^*)p(\theta^*)}{p(N|\theta^{(s)})p(\theta^{(s)})} \tag{13}$$

where r is the acceptance ratio. When we compute r, the following criterion is possible to apply:

- If $r > 1$: since the current damage rate $\theta^{(s)}$ is already accounted for, it meets conventional wisdom to incorporate θ^* which has a higher probability in the pool of fatigue indicator parameters.

If $r < 1$: the current pool already has a higher damage rate probability and for every damage rate, $\theta^{(s)}$ there should be a fraction of θ^*.

Decision: The updated fatigue damage rate $\theta^{(s+1)}$ is equal to the damage rate θ^* or $\theta^{(s)}$ with a frequency of r or $1-r$, respectively.[80]

The Metropolis algorithm progresses by surveying a proposed fatigue damage value θ^* nearby the current value of the damage θ^* using symmetric proposition distribution $J(\theta^*|\theta^{(s)})$, for example, a Gaussian distribution (J designates a symmetric probability distribution). Symmetric here implies that $J(\theta^b|\theta^a) = J(\theta^a|\theta^b)$, that is, the probability of suggesting an updated damage rate $\theta^* = \theta^b$ given that $\theta^{(s)} = \theta^a$ is equal to the probability of suggesting $\theta^* = \theta^a$ given that $\theta^{(s)} = \theta^b$. Usually, $J(\theta^*|\theta^{(s)})$ is very straightforward, with samples from $J(\theta^*|\theta^{(s)})$ being near the sampled damage rates $\theta^{(s)}$ with high probability such that[85]

$$J(\theta^*|\theta^{(s)}) = uniform(\theta^{(s)} - \sigma, \theta^{(s)} + \sigma)$$

$$J(\theta^*|\theta^{(s)}) = normal(\theta^{(s)}, \sigma^2)$$

The amount of standard deviation σ is typically selected to make the estimation algorithm run quickly and effectively; therefore, it is a user-defined parameter. Having obtained a suggested fatigue damage rate θ^*, we add either it or a copy of $\theta^{(s)}$ to the pool of fatigue damage rates, depending on the ratio $r = p(\theta^*|N)/p(\theta^{(s)}|N)$. Specifically, given $\theta^{(s)}$, the Metropolis algorithm for producing an updated fatigue damage rate $\theta^{(s+1)}$ embraces

Sample $\theta^* \sim J(\theta|\theta^{(s)})$

- Calculate the acceptance ratio

$$r = \frac{p(\theta^*|N)}{p(\theta^{(s)}|N)} = \frac{p(N|\theta^*)p(\theta^*)}{p(N|\theta^{(s)})p(\theta^{(s)})}$$

- Respecting

$$\theta^{(s+1)} = \begin{cases} \theta^* & with\ probability\ min(r,1) \\ \theta^{(s)} & with\ probability\ 1 - min(r,1) \end{cases}$$

$min(r,1)$ stems from the fact that probability can be a maximum of 1. The last point can be achieved by surveying $u \sim uniform(0,1)$ and setting $\theta^{(s+1)} = \theta^*$ if $u < r$ and setting $\theta^{(s+1)} = \theta^{(s)}$ alternatively.

Numerical handling

The implementation of the Metropolis algorithm is very similar to the implementation of the general Monte Carlo algorithm. Therefore, here only the part related to the calculation of the acceptance ratio in Equation (13) should be implemented in the program. Additionally, the standard deviation for $J(\theta^*|\theta^{(s)})$ has to be properly conditioned.

2.2.5 | Estimation of error

In Bayesian analysis, the posterior distribution of a fatigue-related influence can be calculated. When a loss of accuracy occurs, the posterior distribution and a loss function may also be used to construct Bayes estimates. A loss function measures the costs of making a certain statistical decision compared with the target fatigue lifetime. The fatigue lifetime squared-error loss function based on the microstructure is

$$L(M, N_f^a) = (M - N_f^a)^2 \tag{14}$$

where M is the microstructure and N_f^a and expected fatigue lifetime. The Bayesian inference analysis aims to minimize the error loss function for the fatigue lifetime. The mean of the posterior distribution of microstructure given a fatigue-related lifetime $\pi(M|N_f^a)$, denoted by M^*, is the Bayes estimate of microstructure M under the squared-error loss function of fatigue lifetime. Furthermore, the absolute error can also give a linear deviation from target fatigue lifetime values. The absolute-error loss function of fatigue lifetime is defined as

$$L(M, N_f^a) = |M - N_f^a| \tag{15}$$

where M is the microstructure and N_f^a and expected fatigue lifetime. The median of the posterior distribution of microstructure given a fatigue-related lifetime $\pi\left(M|N_f^a\right)$, denoted by M^*, is the Bayes estimate of microstructure M under the absolute-error loss function of fatigue lifetime.

3 | RESULTS AND DISCUSSION

3.1 | Transition probabilities

Figure 6 represents the discrete-time, finite-state, time-homogeneous Markov chain from the state transition matrix, based on sampling from the probability distribution of the dendritic width in the Z plane in batch A. We will focus here on this parameter since it was hardly investigated in the literature according to the introduction in this article. It is shown that an immensely high number of transition states is possible within this fatigue damage process with a uniformly distributed transition probability. The property of the Markov chain is unique since it handles the next fatigue damage scenario only based on the present state without memory preservation for historical precedents from the past. In our RL, the training data refresh the algorithm's memory in every calculation iteration. The use of the Markov chain thus prevents any overfitting of the algorithm by the training data since it has no memory from past sequences. Therefore, the Markov property enhances the algorithm's predictive power while avoiding overfitting simultaneously. The transition matrix lists all possible states of the dendrite that may be responsible for fatigue damage initiation. The probability of a specific pass of the trajectory of dendrites during the fatigue damage process will be equal to the product of the initial transition probability and all following single-step transition probabilities. Similar forms of transition probability Markov chains were constructed for porosity, chemical composition, and powder particles. All indicated nonlazy Markov chains without any transition step with a probability higher than 50%.

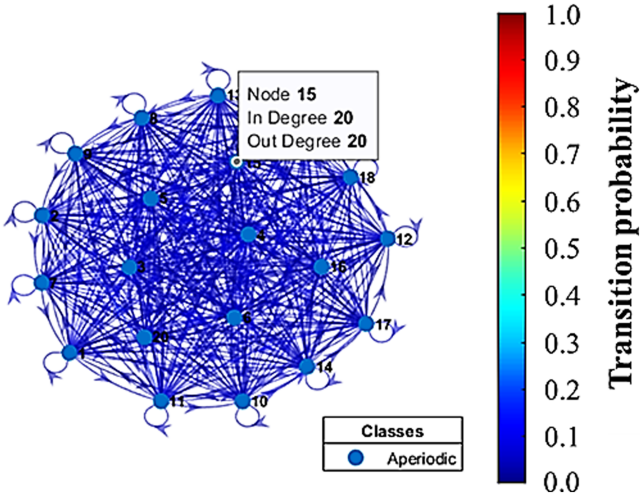

FIGURE 6 Directed graph of the Markov chain with the transition probability for batch A (no PH) based on dendritic width in the Z plane associated with microstructure distribution [Colour figure can be viewed at wileyonlinelibrary.com]

3.2 | Spectral gaps and the convergence rates

The pink disc represents the spectral gap in Figure 7, which is the difference between the two largest eigenvalue moduli.[88] The spectral gap of the eigenvalues of the transition matrix of the Markov chain of dendritic width in the Z plane in batch A is shown in Figure 7. The spectral gap controls the Markov chain's mixing time. Large gaps imply a higher rate of mixing of possible microstructural failure trajectories during fatigue damage, while small gaps suggest a lesser rate of mixing, according to[89]

$$t_{mix}(\epsilon) = \min_{d(t) \le \epsilon} t \tag{16}$$

where t is the mixing time. We experience a nonlazy Markov chain of microstructure here since there is no

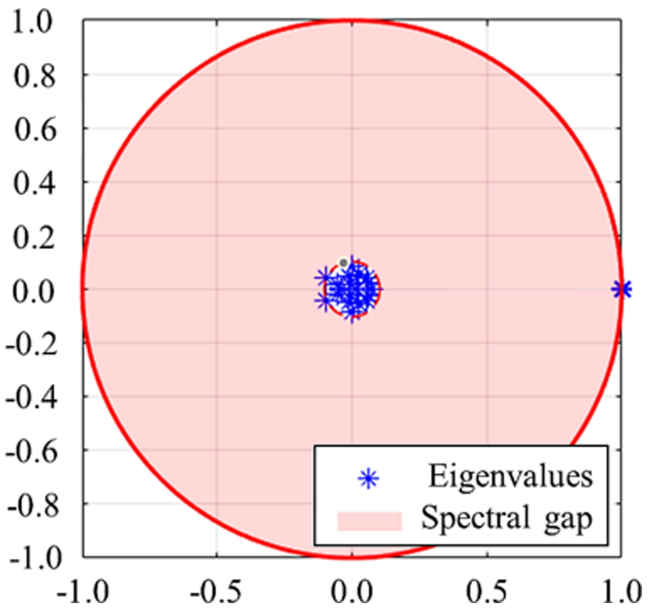

FIGURE 7 Plot of the spectral gap of the eigenvalues of the transition matrix of the Markov chain for batch A (no PH) based on dendritic width in the Z plane associated with microstructure distribution [Colour figure can be viewed at wileyonlinelibrary.com]

probability for any given transition state higher than 50%, according to Figures 6 and 8. Since not all the eigenvalues are positive, the Markov chain is irreversible. The missing time of the Markov chain is naturally occurring here since the spectral gap is unbounded, which means there are no restrictions on the fatigue damage scenarios that can form from all possible trajectories in the sampled microstructure. Therefore, we can sample from the probability distribution of porosity, microstructure, chemical composition, or powder particle size without calculating the normalizing constant by focusing only on the probability ratios of surrounding configurations as in Equation (13).

Figure 8 represents the equilibrium probabilities of the distribution of states of the Markov chain of dendritic damage in the Z plane of batch A according to Grassmann et al.[90] Through this diagram, the finite states of the trajectories of the steps are shown, with state 18 experiencing the highest transitional probability. Since the microstructural fatigue damage process exhibits significant branching, it is necessary to consider the probability of a quasi-finite state only after a significant number of steps where the accepted probability stabilizes.[91] Chikina et al[92] highlighted the uncertainty when the chain would reach a microstructural damage state and a stationary statistical parameter quickly without enough mixing. Therefore, the chain must run for a sufficiently long time. Therefore, we circumvent this here by using the concept developed by Brion et al.,[93] which simply relies on the iterative evaluation of the steady states, resulting in significantly faster accurate conversion with 0.1% accuracy.

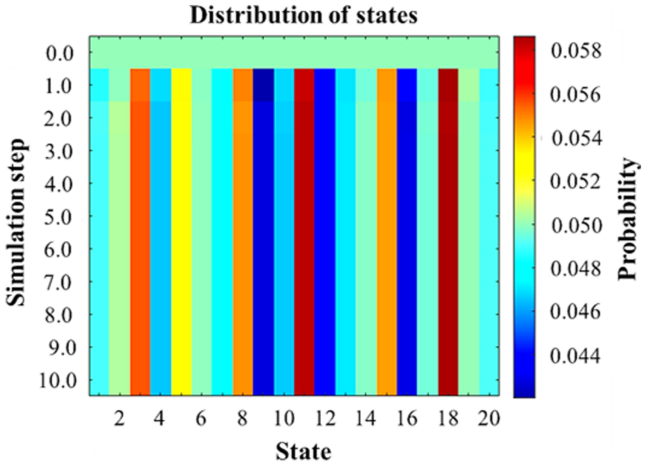

FIGURE 8 Plot of Markov chain distributions for batch A (no PH) based on dendritic width in the Z plane associated with microstructure distribution [Colour figure can be viewed at wileyonlinelibrary.com]

Figure 9 establishes the heatmap of the proportion of simulations of specific states reached by the chain in specific simulation steps. The stationary state of the Markov chain can be used to estimate the transition of the fatigue damage state, as shown by Benasciutti and Tovo.[94] They estimated the transition-cycles rain-flow matrix by the Markov chain. The expected transition from one dendritic width to the other during the fatigue damage or crack propagation process can be stabilized using the Markov chain probability, as Spencer and Tang.[95]

3.3 | Convergence of the acceptance probability

However, as shown earlier, we do not involve a deterministic finite element model here. On the contrary, we are

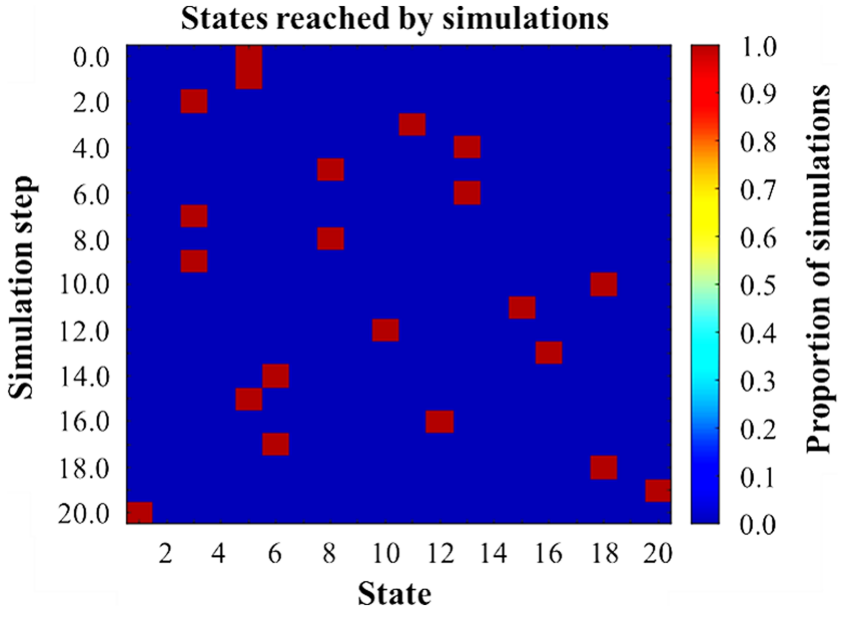

FIGURE 9 Heatmap of the dendritic width of batch A (no PH) in the Z-direction associated with microstructure distribution with random walks through a sequence of damage states in a discrete-time Markov chain [Colour figure can be viewed at wileyonlinelibrary.com]

interested in purely the stationary distribution of the damaged state of the microstructure. A more statistically reliant model on Bayesian statistics was similarly presented by Rastogi et al.,[96] which handled FCG in nuclear piping by aiming to evaluate the posterior distribution using the Markov process. The evolution of state probability and accepted probability is shown in Figure 10. The calculation of accepted probability is based on the acceptance ratio in Equation (13). The concept of accepted probability negates the instability of state probability across withdrawals because of the random sampling in the Monte Carlo process. The accepted probability in the Metropolis Monte Carlo depends exclusively on the random state of the microstructure that is transient in the Markov Chain, according to Creutz.[97] Miller et al.[98] highlighted the importance of achieving a 50% fraction acceptance in the Metropolis process for enough accuracy, although a lower percentage can still be more efficient. Figure 10 achieved a 93% acceptance fraction since, in 93% of the cases, the acceptance ratio of Equation (13) did not update the damage state. In quantum Monte Carlo simulations, Ceperley[99] had to modify step increment to achieve a fraction of acceptance higher than 90%, which is achieved here without adjustment of the steps because of the use of sufficiently dense prior distributions.

Approximately 70% of the available fatigue data was used to train the Monte Carlo (MC) model, while the remaining was used for testing. The grouping was done based on the minimum training data to produce an acceptable accuracy against the testing data. Figure 11 compares the predicted percentiles of the fatigue data and the number of cycles to failure resulting from the fatigue tests. A good agreement between the predicted curve and experimental points across the whole range can be found. Even when the model is handling a physically and fundamentally different mix of data points from the point of view of testing frequency and strain rate, the precision of the model is quite acceptable. This is an inherent advantage of data-driven models, which are nonphenomenological models but could be coupled with mechanistic models to further increase predictive power.[100,101] In a future study, the developed data-driven model here will be coupled with a mechanistic fatigue damage model to elevate the model utility. Worth mentioning that the model presented here has a good character of handling fatigue scatter in the data points even when this scatter is extremely higher in batch A compared with batch B. The scatter in batch B is significantly lower, yet the model shows enough flexibility and adaptive handling for each material condition. This model may be a viable solution for the dispersion problem of testing data in the VHCF regime, which was handled by consideration of heat dissipation.[102] However, using the Metropolis model without extensive experimental data showed good scatter prediction outcomes without

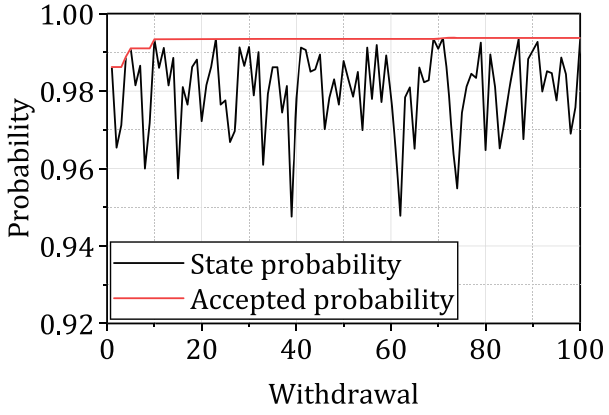

FIGURE 10 Comparison between state probability and accepted probability for 100 withdrawals of the dendritic width of batch A (no PH) in the *Z*-direction associated with microstructure distribution [Colour figure can be viewed at wileyonlinelibrary.com]

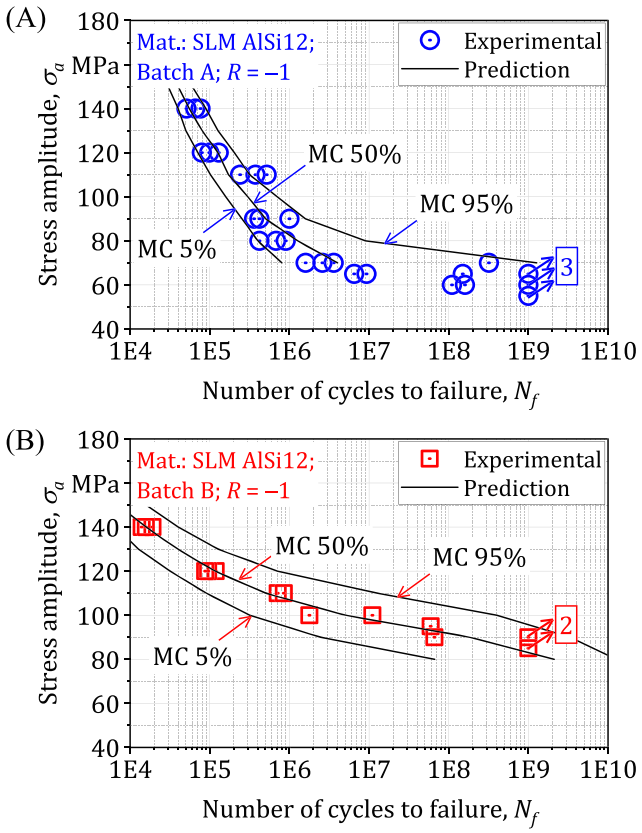

FIGURE 11 Comparison between outcomes of the Monte Carlo (MC) algorithm and the experimental data: (A) Batch A (no PH); (B) Batch B (PH) [Colour figure can be viewed at wileyonlinelibrary.com]

underestimation of scattering; as shown earlier, a simpler Monte Carlo was used.[103] In this study, the Metropolis Monte Carlo algorithm in a Bayesian setting, along with the character of the RL algorithm, promoted the traditional Monte Carlo algorithm to a ML character with sufficient predictive power. It is planned to enhance this power in the future by coupling it with phenomenological modeling and continuum damage theories.[40,41]

3.4 | Predicted influence of heterogeneity on fatigue strength

The strength of the influence of the studied factors on fatigue strength is given in Figure 12. For batch A, the fraction of Al wt.% has the greatest influence on fatigue strength at 120 MPa of stress amplitude, and the dendritic width in the *Z* plane had the lowest influence. The second least influential factor at 120 MPa for batch A was powder particle size. The defect projected area in the Z-direction (load-bearing axis) and the dendritic width in the *XY* plane have closely similar effects. For batch A at 140 MPa, the dendritic width in the *XY* plane is the most influential, while other parameters were similarly less significant. At 120 MPa of stress amplitude, batch B was heavily influenced by powder particle size and dendritic width in the *XY* plane microstructure. Projection of defects in the *Z*-direction, Al wt.%, and *Z* microstructure similarly played a less important role. The combination of Al wt.%, *Z* microstructure, *XY* microstructure, and defect projection in the *Z*-direction was similarly influential for batch B at 140 MPa, while powder particle size played the least significant influence.

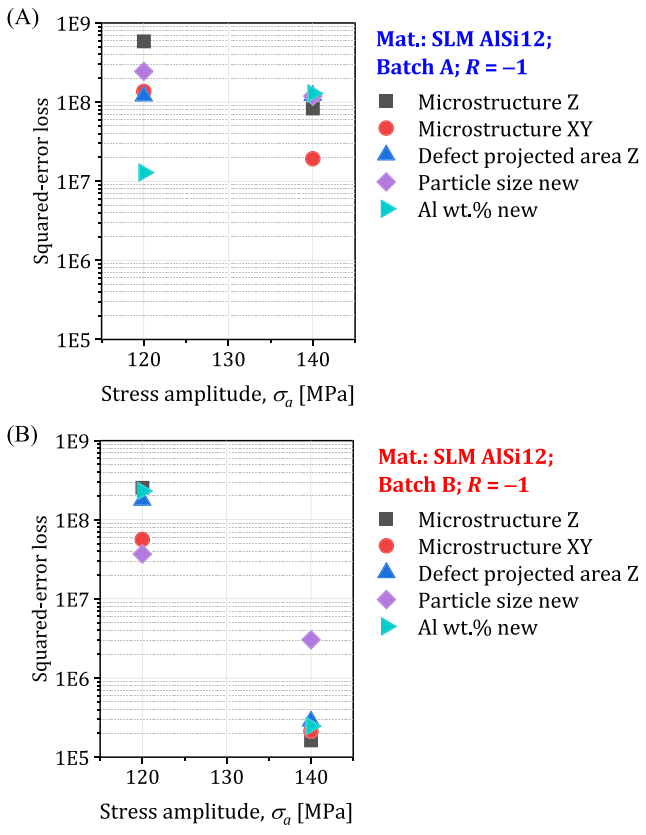

FIGURE 12 Squared-error loss function of the predicted fatigue strength: (A) Batch A (no PH); (B) Batch B (PH) [Colour figure can be viewed at wileyonlinelibrary.com]

Siddique asserted the microstructure's influence on this alloy's fatigue strength in this range of loading.[61] Beretta placed a great emphasis on the projected area and its role in fatigue scatter.[104] We found this particularly true here in Figure 12A. However, second to the influence of chemical composition and microstructure, which does not contradict Berretta[104] or even much earlier statements by Murakami and Endo,[105] who did not discuss these influences in isolation but as secondary influences interacting with the projected area. Schönbauer and Mayer[106] asserted that Murakami and Endo[105] are true if the crack propagation phase highly influences the fatigue strength in sharply notched defects. Biswal et al.[68] confirmed this by stating that below a certain defect size and beyond a certain morphology, retarded short crack behavior undermines the influence of defects on fatigue strength in favor of other factors.

4 | SUMMARY

A reinforcement ML technique is applied to an additively built AlSi12 alloy using Bayesian inferential statistics and the Metropolis Monte Carlo algorithm. The aim was to determine the posterior distributions of fatigue strength. This research aims to determine the effect of structural heterogeneity on extremely HCF strength in AM. To produce specimens from AlSi12 powder, a laser beam melting system was employed. The device was equipped with a 400 W fiber laser capable of deposition platform temperatures up to 200°C. A cluster of pores precipitated the failure in the specimen's immediate subsurface. The failure did not begin with the biggest or most asymmetrical flaw. Monte Carlo techniques and processes may help build a posterior estimate of fatigue strength using a simulation-based inference technique. The Markov property of the Markov chain is unique in that it determines the next scenario of fatigue damage only based on the current state. The heatmap showed the equilibrium probability of the distribution of states of the Markov chain of dendritic. Large gaps suggest a faster mixing of microstructural failure paths during fatigue damage. The

acceptable probability in Metropolis Monte Carlo is entirely dependent on the random state of the microstructure that is transitory in the Markov chain. A 93% fraction acceptance achieved sufficient precision without tunning. The model offered a potential solution to the dispersion issue associated with testing data in the VHCF regime. The fraction of chemical composition was shown to significantly influence fatigue strength in addition to traditionally discussed influences such as projected area, which is of higher significance if fatigue lifetime in crack propagation is dominant.

ACKNOWLEDGMENTS

The authors thank the German Research Foundation (Deutsche Forschungsgemeinschaft, DFG) for its financial support within the research project "Mechanism-based understanding of functional grading focused on fatigue behavior of additively processed Ti-6Al-4V and Al-12Si alloys" (WA 1672/25-1). The authors further thank Fraunhofer IAPT, Hamburg, for providing the samples in the framework of excellent scientific collaboration. Open Access funding enabled and organized by Projekt DEAL.

DATA AVAILABILITY STATEMENT

Research data are not shared.

NOMENCLATURE

N	Number of cycles
$\Delta\sigma$	Stress range
β	Shape parameter
δ	Scale parameter
B	Fatigue lifetime threshold
C	Fatigue strength threshold
P_z	Projected area in the Z-direction
d_p	Pore diameter
σ_a	Stress amplitude
N_f	Number of cycles to failure
$f_{\cdot}(N, \Delta\sigma)$	Lifetime and stress range conjugates
N	Sampled number of cycles
N	Sampled fatigue lifetime
θ^f	True mean failure rate
S	Sample
Ψ_n	Random fatigue damage state
r	Acceptance ratio
σ	Deviation
M	Microstructure sample
N_f^a	Expected fatigue lifetime
$\pi\left(M\middle\vert N_f^a\right)$	Posterior distribution of microstructure given a fatigue-related lifetime
t	Mixing time in the Markov chain

ORCID

Mustafa Awd https://orcid.org/0000-0002-9404-0067

REFERENCES

1. Dimiduk DM, Holm EA, Niezgoda SR. Perspectives on the impact of machine learning, deep learning, and artificial intelligence on materials, processes, and structures engineering. *Integr Mater Manuf Innov*. 2018;7(3):157-172.
2. Sha W, Guo Y, Yuan Q, et al. Artificial intelligence to power the future of materials science and engineering. *Adv Intell Syst*. 2020;2(4):1900143.
3. Bzdok D, Altman N, Krzywinski M. Statistics versus machine learning. *Nat Methods*. 2018;15(4):233-234.
4. Zhou L, Pan S, Wang J, Vasilakos AV. Machine learning on big data: opportunities and challenges. *Neurocomputing*. 2017; 237:350-361.
5. Ruotsalainen M, Jylhä J, Visa A. Minimizing fatigue damage in aircraft structures. *IEEE Intell Syst*. 2016;31(4):22-29.
6. Farrar CR, Worden K. *Structural health monitoring: A machine learning perspective*. Chichester, West Sussex, U.K.; Hoboken, N.J: Wiley; 2012.
7. Dervilis N, Choi M, Antoniadou I, et al. Machine learning applications for a wind turbine blade under continuous fatigue loading. *Key Eng Mater*. 2013;588:166-174.
8. Qi X, Chen G, Li Y, Cheng X, Li C. Applying neural-network-based machine learning to additive manufacturing: current applications, challenges, and future perspectives. *Engineering*. 2019;5(4):721-729.
9. Wang Z, Liu J, Zhang Y, Yuan H, Zhang R, Srinivasan RS. Practical issues in implementing machine-learning models for building energy efficiency: moving beyond obstacles. *Renew Sustain Energy Rev*. 2021;143:110929.
10. Johnson NS, Vulimiri PS, To AC, et al. Invited review: machine learning for materials developments in metals additive manufacturing. *Addit Manuf*. 2020;36:101641.
11. Allam O, Holmes C, Greenberg Z, Kim KC, Jang SS. Density functional theory—machine learning approach to analyze the bandgap of elemental halide perovskites and ruddlesden-popper phases. *ChemPhysChem*. 2018;19(19):2559-2565.
12. Williamson A, Lombardi DA, Folkard S, Stutts J, Courtney TK, Connor JL. The link between fatigue and safety. *Accid Anal Prev*. 2011;43(2):498-515.
13. Kong X, Zhang Z, Meng L, Tomiyama H. Machine learning based features matching for fatigue crack detection. *Proc Comput Sci*. 2020;174:101-105.
14. Kumar A. Computer-vision-based fabric defect detection: a survey. *IEEE Trans Ind Electron*. 2008;55(1):348-363.
15. Zhang L, Wang Z, Wang L, Zhang Z, Chen X, Meng L. Machine learning based real-time visible fatigue crack growth detection. *Digit Commun Netw*. 2021;7(4):551-558.
16. Kamble RG, Raykar NR, Jadhav DN. Machine learning approach to predict fatigue crack growth. *Mater Today Proc*. 2021;38:2506-2511.
17. Schijve J. *Fatigue of structures and materials*. Second ed. Dordrecht: Springer; 2009.
18. Durodola JF, Ramachandra S, Gerguri S, Fellows NA. Artificial neural network for random fatigue loading analysis including the effect of mean stress. *Int J Fatigue*. 2018;111:321-332.

19. Celikoglu HB. Application of radial basis function and generalized regression neural networks in non-linear utility function specification for travel mode choice modelling. *Math Comput Model*. 2006;44(7-8):640-658.
20. Zhang M, Sun C-N, Zhang X, et al. High cycle fatigue life prediction of laser additive manufactured stainless steel: a machine learning approach. *Int J Fatigue*. 2019;128:105194.
21. Huang DJ, Li H. A machine learning guided investigation of quality repeatability in metal laser powder bed fusion additive manufacturing. *Mater Des*. 2021;203:109606.
22. Nowell D, Nowell PW. A machine learning approach to the prediction of fretting fatigue life. *Tribol Int*. 2020;141:105913.
23. Ahmad HW, Hwang JH, Javed K, Chaudry UM, Bae DH. Probabilistic fatigue life prediction of dissimilar material weld using accelerated life method and neural network approach. *Computation*. 2019;7:10.
24. Hu D, Su X, Liu X, Mao J, Shan X, Wang R. Bayesian-based probabilistic fatigue crack growth evaluation combined with machine-learning-assisted GPR. *Eng Fract Mech*. 2020;229:106933.
25. Chen J, Liu Y. Probabilistic physics-guided machine learning for fatigue data analysis. *Expert Syst Appl*. 2021;168:114316.
26. Zhan Z, Li H. A novel approach based on the elastoplastic fatigue damage and machine learning models for life prediction of aerospace alloy parts fabricated by additive manufacturing. *Int J Fatigue*. 2021;145:106089.
27. He L, Wang Z, Akebono H, Sugeta A. Machine learning-based predictions of fatigue life and fatigue limit for steels. *J Mater Sci Technol*. 2021;90:9-19.
28. Zhan Z, Hu W, Meng Q. Data-driven fatigue life prediction in additive manufactured titanium alloy: a damage mechanics based machine learning framework. *Eng Fract Mech*. 2021;252:107850.
29. Di Maio F, Tsui KL, Zio E. Combining relevance vector machines and exponential regression for bearing residual life estimation. *Mech Syst Signal Process*. 2012;31:405-427.
30. Gan L, Zhao X, Wu H, Zhong Z. Estimation of remaining fatigue life under two-step loading based on kernel-extreme learning machine. *Int J Fatigue*. 2021;148:106190.
31. Narasimharaju SR, Zeng W, See TL, et al. A comprehensive review on laser powder bed fusion of steels: processing, microstructure, defects and control methods, mechanical properties, current challenges and future trends. *J Manuf Process*. 2022;75:375-414.
32. Bao H, Wu S, Wu Z, Kang G, Peng X, Withers PJ. A machine-learning fatigue life prediction approach of additively manufactured metals. *Eng Fract Mech*. 2021;242:107508.
33. Luo YW, Zhang B, Feng X, et al. Pore-affected fatigue life scattering and prediction of additively manufactured Inconel 718: an investigation based on miniature specimen testing and machine learning approach. *Mater Sci Eng A Struct Mater*. 2021;802:140693.
34. Chen T, Guestrin C. XGBoost: A scalable tree boosting system. In: *Proceedings of the 22nd ACM SIGKDD*. San Francisco California USA: ACM; 2016:785-794.
35. Ke G, Meng Q, Finley T, et al. LightGBM: A highly efficient gradient boosting decision tree. In: Guyon I, Luxburg UV, Bengio S, et al., eds. *Advances in neural information processing systems*, Vol. 30. Curran Associates, Inc.; 2017.
36. Mirjalili S, Saremi S, Mirjalili SM, Coelho LDS. Multi-objective grey wolf optimizer: a novel algorithm for multi-criterion optimization. *Expert Syst Appl*. 2016;47:106-119.
37. Movsessian A, Cava DG, Tcherniak D. Interpretable machine earning in damage detection using Shapley additive explanations. *ASCE-ASME J Risk Uncertain Eng Syst A Civ Eng*. 2022;8:021101.
38. Yan F, Song K, Liu Y, Chen S, Chen J. Predictions and mechanism analyses of the fatigue strength of steel based on machine learning. *J Mater Sci*. 2020;55(31):15334-15349.
39. Al-Abbasi FM, Nemes JA. Micromechanical modeling of dual phase steels. *Int J Mech Sci*. 2003;45(9):1449-1465.
40. Reimann D, Nidadavolu K, ul Hassan H, et al. Modeling macroscopic material behavior with machine learning algorithms trained by micromechanical simulations. *Front Mater*. 2019;6:181.
41. Zhan Z, Li H. Machine learning based fatigue life prediction with effects of additive manufacturing process parameters for printed SS 316L. *Int J Fatigue*. 2021;142:105941.
42. Jang D-W, Lee S, Park J-W, Baek D-C. Failure detection technique under random fatigue loading by machine learning and dual sensing on symmetric structure. *Int J Fatigue*. 2018;114:57-64.
43. Sysyn M, Gerber U, Nabochenko O, Gruen D, Kluge F. Prediction of rail contact fatigue on crossings using image processing and machine learning methods. *Urban Rail Transit*. 2019;5(2):123-132.
44. Ukai K, Rahman R, Yagi N, et al. Detecting pelvic fracture on 3D-CT using deep convolutional neural networks with multi-orientated slab images. *Sci Rep*. 2021;11(1):11716.
45. Eberbeck D, Wiekhorst F, Wagner S, Trahms L. How the size distribution of magnetic nanoparticles determines their magnetic particle imaging performance. *Appl Phys Lett*. 2011;98(18):182502.
46. Wang SY, Zhang PZ, Zhou SY, Wei DB, Ding F, Li FK. A computer vision based machine learning approach for fatigue crack initiation sites recognition. *Comput Mater Sci*. 2020;171:109259.
47. MacAllister A, Kohl A, Winer E. Using high-fidelity metamodels to improve performance of small dataset trained Bayesian networks. *Expert Syst Appl*. 2020;139:112830.
48. Choi J, Quagliato L, Lee S, Shin J, Kim N. Multiaxial fatigue life prediction of polychloroprene rubber (CR) reinforced with tungsten nano-particles based on semi-empirical and machine learning models. *Int J Fatigue*. 2021;145:106136.
49. Zhuang Y, Qin J, Chen B, Dong C, Xue C, Easa SM. Data loss reconstruction method for a bridge weigh-in-motion system using generative adversarial networks. *Sensors*. 2022;22(3):858.
50. Deng Y, Zhang M, Feng D-M, Li A-Q. Predicting fatigue damage of highway suspension bridge hangers using weigh-in-motion data and machine learning. *Struct Infra Eng*. 2021;17(2):233-248.
51. Hejazi R, Grime A, Randolph M, Efthymiou M. A Bayesian machine learning approach to rapidly quantifying the fatigue probability of failure for steel catenary risers. *Ocean Eng*. 2021;235:109353.
52. Barto A, Duff M. Monte Carlo matrix inversion and reinforcement learning. In: Cowan J, Tesauro G, Alspector J, eds.

Advances in neural information processing systems, Vol. 6. Morgan-Kaufmann; 1993.
53. Tomita Y, Shiina K, Okabe Y, Lee HK. Machine-learning study using improved correlation configuration and application to quantum Monte Carlo simulation. *Phys Rev E*. 2020; 102(2):021302.
54. Weinan E, Han J, Jentzen A. Algorithms for solving high dimensional PDEs: from nonlinear Monte Carlo to machine learning. *Nonlinearity*. 2021;35:278.
55. Foreman S, Jin X-Y, Osborn JC. Deep learning Hamiltonian Monte Carlo. In: *ICLR 2021 SimDL Workshop*. arXiv; 2021.
56. Walpole RE, Myers RH, Myers SL, Ye K. *Probability & Statistics for Engineers & Scientists: MyStatLab* Update 2017.
57. Castillo E, Fernández-Canteli A. *A unified statistical methodology for modeling fatigue damage*. Dordrecht: Springer; 2009.
58. Siddique S, Awd M, Tenkamp J, Walther F. Development of a stochastic approach for fatigue life prediction of AlSi12 alloy processed by selective laser melting. *Eng Fail Anal*. 2017;79: 34-50.
59. Siddique S, Imran M, Wycisk E, Emmelmann C, Walther F. Influence of process-induced microstructure and imperfections on mechanical properties of AlSi12 processed by selective laser melting. *J Mater Process Technol*. 2015;221:205-213.
60. Siddique S, Imran M, Walther F. Very high cycle fatigue and fatigue crack propagation behavior of selective laser melted AlSi12 alloy. *Int J Fatigue*. 2017;94:246-254.
61. Siddique S. *Reliability of selective laser melted AlSi12 alloy for quasistatic and fatigue applications*. Wiesbaden: Springer Fachmedien Wiesbaden; 2019.
62. Siddique S, Imran M, Rauer M, et al. Computed tomography for characterization of fatigue performance of selective laser melted parts. *Mater Des*. 2015;83:661-669.
63. Awd M, Siddique S, Johannsen J, Emmelmann C, Walther F. Very high-cycle fatigue properties and microstructural damage mechanisms of selective laser melted AlSi10Mg alloy. *Int J Fatigue*. 2019;124:55-69.
64. Prashanth KG, Scudino S, Klauss HJ, et al. Microstructure and mechanical properties of Al–12Si produced by selective laser melting: effect of heat treatment. *Mater Sci Eng A Struct Mater*. 2014;590:153-160.
65. Aboulkhair NT, Maskery I, Tuck C, Ashcroft I, Everitt NM. Improving the fatigue behaviour of a selectively laser melted aluminium alloy: influence of heat treatment and surface quality. *Mater Des*. 2016;104:174-182.
66. Solberg K, Guan S, Razavi SMJ, Welo T, Chan KC, Berto F. Fatigue of additively manufactured 316L stainless steel: the influence of porosity and surface roughness. *Fatigue Fract Eng Mater Struct*. 2019;42(9):2043-2052.
67. Collins PC, Brice DA, Samimi P, Ghamarian I, Fraser HL. Microstructural control of additively manufactured metallic materials. *Annu Rev Mat Res*. 2016;46(1):63-91.
68. Biswal R, Zhang X, Shamir M, et al. Interrupted fatigue testing with periodic tomography to monitor porosity defects in wire+arc additive manufactured Ti-6Al-4V. *Addit Manuf*. 2019;28:517-527.
69. Biswal R, Zhang X, Syed AK, et al. Criticality of porosity defects on the fatigue performance of wire+arc additive manufactured titanium alloy. *Int J Fatigue*. 2019;122:208-217.
70. Awd M, Labanie MF, Moehring K, Fatemi A, Walther F. Towards deterministic computation of internal stresses in additively manufactured materials under fatigue loading: part I. *Materials*. 2020;13(10):2318.
71. Awd M, Siddique S, Walther F. Microstructural damage and fracture mechanisms of selective laser melted Al-Si alloys under fatigue loading. *Theor Appl Fract Mech*. 2020;106: 102483.
72. Maltamo M, Kangas A, Uuttera J, Torniainen T, Saramäki J. Comparison of percentile based prediction methods and the Weibull distribution in describing the diameter distribution of heterogeneous scots pine stands. *For Ecol Manage*. 2000; 133(3):263-274.
73. Awd M, Siddique S, Hajavifard R, Walther F. Comparative study of defect-based and plastic damage-based approaches for fatigue lifetime calculation of selective laser melted AlSi12. In: Abdel Wahab M, ed. *Proceedings of the 7th international conference on fracture fatigue and wear*. Lecture Notes in Mechanical Engineering. Singapore: Springer Singapore; 2019:297-313.
74. Awd M, Walther F, Siddique S, Fatemi A. Microstructure and fatigue damage evolution in additive-manufactured metals using enhanced measurement techniques and modeling approaches. In: The Minerals, Metals & Materials Society, ed. *TMS 2021 150th annual meeting & exhibition supplemental proceedings*. The Minerals, Metals & Materials Series. Cham: Springer International Publishing; 2021:753-762.
75. McDowell DL, Dunne FPE. Microstructure-sensitive computational modeling of fatigue crack formation. *Int J Fatigue*. 2010;32(9):1521-1542.
76. Siddique S, Awd M, Tenkamp J, Walther F. High and very high cycle fatigue failure mechanisms in selective laser melted aluminum alloys. *J Mater Res*. 2017;32(23):4296-4304.
77. Tridello A, Fiocchi J, Biffi CA, et al. Influence of the annealing and defects on the VHCF behavior of an SLM AlSi10Mg alloy. *Fatigue Fract Eng Mater Struct*. 2019;42(12):2794-2807.
78. Robert CP, Casella G. *Monte Carlo statistical methods*. Vol. 2010. 2nd ed, softcover reprint of the hardcover 2. ed. New York, NY: Springer New York; 2004.
79. Spanos PD, Wu Y-T. *Probabilistic structural mechanics: Advances in structural reliability methods*. Berlin, Heidelberg: Springer Berlin Heidelberg; 1994.
80. Hoff PD. *A first course in Bayesian statistical methods*. London; New York: Springer; 2009.
81. Sobczyk K. *Stochastic approach to fatigue: Experiments, modelling and reliability estimation*. Vienna: Springer Wien; 2014.
82. Awd M, Johannsen J, Chan T, Merghany M, Emmelmann C, Walther F. Improvement of fatigue strength in lightweight selective laser melted alloys by in situ and ex situ composition and heat treatment. In: The Minerals, Metals & Materials Society, ed. *TMS 2020 149th annual meeting & exhibition supplemental proceedings*. The Minerals, Metals & Materials Series. Cham: Springer International Publishing; 2020: 115-126.
83. Xu W, Brandt M, Sun S, et al. Additive manufacturing of strong and ductile Ti–6Al–4V by selective laser melting via in situ martensite decomposition. *Acta Mater*. 2015;85:74-84.

84. Robert C. *The Bayesian choice: From decision-theoretic foundations to computational implementation*. 2nd ed. New York: Springer; 2007.
85. Cowles MK. *Applied Bayesian statistics: with R and OpenBUGS examples*. New York: Springer; 2013.
86. Privault N. *Understanding Markov chains: Examples and applications*, Vol. 2018. 2nd ed. Singapore: Springer Singapore: Imprint: Springer; 2018.
87. Limnios N, Oprişan G. *Semi-Markov processes and reliability*. Boston, MA: Birkhäuser; 2001.
88. Gallager RG. *Stochastic processes: Theory for Applications*. Cambridge, United Kingdom; New York: Cambridge University Press; 2013.
89. Boyd S, Diaconis P, Parrilo PA, Xiao L. Fastest mixing Markov chain on graphs with symmetries. *SIAM J Control Optim*. 2007;20(2):792-819.
90. Grassmann WK, Taksar MI, Heyman DP. Regenerative analysis and steady state distributions for Markov chains. *Oper Res*. 1985;33(5):1107-1116.
91. Seneta E, Vere-Jones D. On quasi-stationary distributions in discrete-time Markov chains with a denumerable infinity of states. *J Appl Probab*. 1966;3(2):403-434.
92. Chikina M, Frieze A, Pegden W. Assessing significance in a Markov chain without mixing. *Proc Natl Acad Sci*. 2017; 114(11):2860-2864.
93. Feinberg BN, Chiu SS. A method to calculate steady-state distributions of large Markov chains by aggregating states. *Oper Res*. 1987;35(2):282-290.
94. Benasciutti D, Tovo R. On fatigue cycle distribution in non-stationary switching loadings with Markov chain structure. *Prob Eng Mech*. 2010;25(4):406-418.
95. Spencer BF, Tang J. Markov process model for fatigue crack growth. *J Eng Mech*. 1988;114(12):2134-2157.
96. Rastogi R, Ghosh S, Ghosh AK, Vaze KK, Singh PK. Fatigue crack growth prediction in nuclear piping using Markov chain Monte Carlo simulation. *Fatigue Fract Eng Mater Struct*. 2017; 40(1):145-156.
97. Creutz M. Overrelaxation and Monte Carlo simulation. *Phy Rev D*. 1987;36(2):515-519.
98. Miller MA, Amon LM, Reinhardt WP. Should one adjust the maximum step size in a Metropolis Monte Carlo simulation? *Chem Phys Lett*. 2000;331(2-4):278-284.
99. Ceperley DM. Metropolis methods for quantum Monte Carlo simulations. In: *AIP conference proceedings*. Vol. 690. Los Alamos, New Mexico (USA): AIP; 2003:85-98.
100. Bellotti M, Wu M, Qian J, Reynaerts D. Tool wear and material removal predictions in micro-EDM drilling: advantages of data-driven approaches. *Appl Sci*. 2020;10(18):6357.
101. Tsopanoglou A, Jiménez del Val I. Moving towards an era of hybrid modelling: advantages and challenges of coupling mechanistic and data-driven models for upstream pharmaceutical bioprocesses. *Curr Opin Chem Eng*. 2021;32:100691.
102. Huang ZY, Wang QY, Wagner D, Bathias C, Chaboche JL. A rapid scatter prediction method for very high cycle fatigue: a rapid scatter prediction for VHCF. *Fatigue Fract Eng Mater Struct*. 2013;36(5):462-468.
103. El Khoukhi D, Morel F, Saintier N, Bellett D, Osmond P, Le V-D. Probabilistic modeling of the size effect and scatter in high cycle fatigue using a Monte-Carlo approach: role of the defect population in cast aluminum alloys. *Int J Fatigue*. 2021; 147:106177.
104. Beretta S. More than 25 years of extreme value statistics for defects: fundamentals, historical developments, recent applications. *Int J Fatigue*. 2021;151:106407.
105. Murakami Y, Endo M. Effects of defects, inclusions and inhomogeneities on fatigue strength. *Int J Fatigue*. 1994;16(3): 163-182.
106. Schönbauer BM, Mayer H. Effect of small defects on the fatigue strength of martensitic stainless steels. *Int J Fatigue*. 2019;127:362-375.

How to cite this article: Awd M, Münstermann S, Walther F. Effect of microstructural heterogeneity on fatigue strength predicted by reinforcement machine learning. *Fatigue Fract Eng Mater Struct*. 2022;45(11): 3267-3287. doi:10.1111/ffe.13816